

The Relationship of Source Parameters of Oceanic Transform Earthquakes to Plate Velocity and Transform Length

NORMAN C. BURR AND SEAN C. SOLOMON

Department of Earth and Planetary Sciences, Massachusetts Institute of Technology, Cambridge, Massachusetts 02139

The source parameters of large earthquakes on oceanic transform faults are closely related to the thermal and mechanical properties of oceanic lithosphere. Several characteristics of these earthquakes (including magnitude, moment, and apparent stress $\eta\bar{\sigma}$) are synthesized according to local plate velocity V , ridge-ridge offset L , and average fault width W estimated by Brune's method. Several relationships result: (1) the maximum moment M_0 on a transform decreases with V , (2) maximum M_0 appears to increase with L for $L < 400$ km and may decrease for greater offsets, (3) $\eta\bar{\sigma}$ does not clearly depend on either V or L , (4) the maximum estimated $W(V)$ decreases with V , (5) the minimum estimated $W(L)$ increases with L , and (6) the largest earthquakes on long transforms occur near the transform center. Most of these relationships are consistent with the hypothesis that seismic failure occurs only at temperatures below a fixed value. An inversion of slip rate and magnitude data by transform supports this hypothesis and gives an estimate for the nominal temperature of the boundary separating stick slip and stable sliding. Though the actual thermal structure around oceanic transforms is not known, the idealized spreading plate models used in the inversion give a temperature range for the brittle to ductile boundary of 75°–150°C. If possible uncertainties in the thermal structure are allowed for, a range of 50°–300°C provides a conservative bound on the true limiting temperature. These temperature ranges are consistent with focal depths of transform earthquakes and with laboratory measurements of fault slip in rocks of compositions that are representative candidates for the material being faulted in oceanic transforms.

INTRODUCTION

A transform fault is a segment of a plate boundary along which the two plates are in strike slip relative motion [Wilson, 1965; Sykes, 1967]. On oceanic spreading center systems the largest earthquakes occur on the transforms rather than on the ridge axes [Isacks *et al.*, 1968]. Probably all spreading center earthquakes with $M > 7$ in the Gutenberg and Richter [1954] catalog, for instance, are transform events; the largest such events in their list are $M \approx 8$.

What properties control the size of an earthquake occurring on a given transform? Clearly, the spreading rate is important, as is the total offset of the transform. These parameters in turn control the age of the lithosphere on both sides of the transform that may participate in the faulting. Is age, and thus thermal structure, the controlling variable? or is transform offset? or slip rate? This paper addresses these questions.

The source parameters of earthquakes on over 60 oceanic transforms are synthesized according to transform length and spreading rate. The hypothesis is developed that for most large transform events the depth of seismic failure is limited by a single fixed isotherm (Figure 1). The hypothesis is tested by inverting slip rate and magnitude data for the set of transforms to find the limiting temperature consistent with available moment-magnitude information for transform earthquakes. The test supports the idea that thermal structure is the main control on earthquake size and gives a nominal value for the limiting temperature of $100^\circ \pm 50^\circ\text{C}$, a figure that has considerable uncertainty because of the complicated thermal structure of actual transform faults. Both focal depth data for transform earthquakes and laboratory measurements of the temperature marking the boundary between stick slip and stable sliding behavior are consistent with the results of the inversion. A few very large transform earthquakes are not consistent with the limiting temperature hypothesis as quantified by the inversion results; some comments on the possible origin of this inconsistency are offered.

SOME DEFINITIONS

There are several terms which will be referred to frequently and therefore warrant definition. A transform, that region between offset ridge crests along which active slip occurs [Wilson, 1965], is characterized by a length L , the distance between ridge crest segments, and a width W , the depth above which brittle failure occurs. The true width may not be constant along the transform, so that W represents an average depth.

The term fault will refer to the area, taken to be rectangular, over which seismic slip occurs during a single earthquake. A fault has a length l , which is not usually equal to the transform length except in the cases of very short transforms or very large earthquakes, and a width w , which may correspond to the transform width.

Two measures of earthquake size are the magnitude and the moment. The magnitude is taken to be the standard 20-s surface wave magnitude of Gutenberg and Richter [1942] or its equivalent. The seismic moment M_0 of an earthquake can be related [Aki, 1966] to fault area lw and to the average displacement \bar{d} by

$$M_0 = \mu l w \bar{d} \quad (1)$$

where μ is the shear modulus.

Another useful concept is the moment sum $\sum M_0$, which is the sum of the moments for all earthquakes on a given transform within a specified time period. The moment sum can be related to the transform area $A = LW$ by

$$\sum M_0 = \mu A V T \quad (2)$$

[Brune, 1968; Davies and Brune, 1971], where V is the slip rate or full spreading velocity at the ridge and T is the time interval over which the summation is taken. This equation is based on the assumptions that all slip on the transform to depth W is accomplished by brittle failure and that the time interval T is sufficiently long to obtain a representative sample of large earthquakes.

Two useful measures of the shear stress acting during seismic failure are the apparent stress $\eta\bar{\sigma}$ and the stress drop $\Delta\sigma$.

Approved for public release
distribution unlimited.

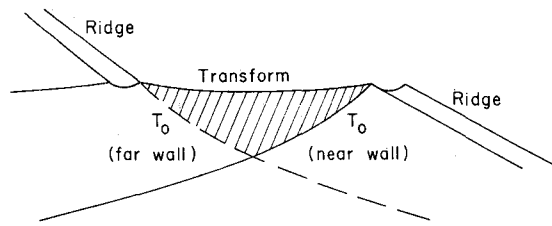


Fig. 1. Schematic view of how an isotherm may limit the area of a transform susceptible to seismic failure.

The apparent stress is the product of the average shear stress $\bar{\sigma}$ on the fault before and after faulting and an unknown efficiency factor η . The stress drop is the difference between the initial and the final shear stress on the fault. The apparent stress may be calculated for an earthquake from the relation [Aki, 1966]

$$\eta\bar{\sigma} = \mu E/M_0 \quad (3)$$

where E is the radiated seismic energy. The energy E is commonly estimated from either the body wave magnitude m_b or the surface wave magnitude M_s , by using either

$$\log_{10} E = 5.8 + 2.4m_b \quad (4)$$

or

$$\log_{10} E = 11.8 + 1.5M_s \quad M_s \geq 6\frac{1}{2} \quad (5)$$

[Gutenberg and Richter, 1956]. Apparent stresses derived from (3) will be designated $\eta\bar{\sigma}_b$ or $\eta\bar{\sigma}_s$ if equation (4) or (5), respectively, is used to estimate E . The stress drop may be calculated if the seismic moment and fault shape are known [Knopoff, 1958]:

$$\Delta\sigma = 2M_0/\pi lw^2 \quad (6)$$

TRANSFORM DATA

The population of oceanic transforms considered in this study consists of those satisfying two criteria: (1) each is sufficiently well surveyed that both the location and the transform length are known, and (2) on each has occurred at least one magnitude 6 or greater earthquake according to the catalogs of Gutenberg and Richter [1954] and the U.S. Geological Survey (USGS).

Sixty oceanic transforms satisfy these two criteria and are listed in Table 1. The sources of bathymetric and seismicity information on transform location and length include Anderson and Sclater [1972], Anderson et al. [1974], Bonatti and Honnorez [1976], Collette et al. [1974], Fisher et al. [1971], Forsyth [1972, 1975], Fox et al. [1976], Herron [1972a], Klitgord et al. [1973], Mammerickx et al. [1975], McKenzie and Sclater [1971], Molnar et al. [1975], Norton [1976], Olivet et al. [1974], Sclater and Fisher [1974], Sclater et al. [1976], Sykes [1967], Thompson and Melson [1972], van Andel et al. [1973], Vogt and Johnson [1975], and Weissel and Hayes [1972]. Uncertainties in the estimates of L from inspection of published maps vary but are generally less than 15%. The spreading rates for each transform are calculated from model RM1 of Minster et al. [1974].

The list in Table 1 includes most of the large midoceanic transforms except for two exceptional regions: the African-Antarctic plate boundary and the complicated zones on the east Pacific rise near 20°S and 34°S [Herron, 1972b]. Further

survey work in these areas is a prerequisite for their inclusion in future studies of this type. A few well-surveyed transforms in regions of currently changing plate motions (e.g., Mendocino, Rivera) were also excluded. The requirement for an $M = 6$ earthquake eliminates transforms shorter than 70- to 80-km length.

One transform on the African-Antarctic plate boundary has been included in Table 1 because it marks the occurrence of the largest earthquake on any spreading center system: an $M = 7.9$ event on November 10, 1942, at 49°S, 32°E [Gutenberg and Richter, 1954]. Though the geometry of this unusual transform is not known well, Norton [1976] has verified the strike slip nature of the local plate motion and has suggested a transform length of up to 400 km.

EARTHQUAKE DATA

The history of $M \geq 6$ earthquake activity on each of the transforms in Table 1 has been compiled from several catalogs and is listed by Burr [1977]. Earthquakes and magnitudes for 1912-1952 are from Gutenberg and Richter [1954], for 1953-1965 are from Rothé [1969], and for 1966-1975 are generally from the U.S. Coast and Geodetic Survey, NOAA, and USGS. Geller and Kanamori [1977] have shown that the magnitude M of Gutenberg and Richter is similar to the modern 20-s surface wave magnitude. The assumption is made that the magnitudes from Rothé [1969] are also on a comparable scale.

For many of the large transform earthquakes since 1963, seismic source parameters other than magnitude are available from the spectral analysis of seismic body and surface waves. Seismic moments have been reported in the literature for 30 transform events [Brune and King, 1967; Brune, 1968; Tsai, 1969; Wyss, 1970; Udias, 1971; Weidner and Aki, 1973; Forsyth, 1973; Kanamori and Stewart, 1976]; these earthquakes are listed in Table 2.

Also given in Table 2 are newly determined moments for six additional transform earthquakes, four in the South Pacific [Molnar et al., 1975] and two on the southwest Indian ridge [Norton, 1976]. The moments were determined from the long-period spectral amplitudes of SH waves recorded at 4-7 World-Wide Standard Seismograph Network stations for each event. Corrections for instrument, radiation pattern, free surface at source and receiver, geometrical spreading, and attenuation follow Richardson and Solomon [1977]. Spectra for all events are given by Burr [1977].

Apparent stresses for each event are given in Table 2, by using either (4) or (5). The apparent stresses determined either from m_b or M_s are comparable to apparent stresses for other types of plate boundary earthquakes and for intraplate events [Richardson and Solomon, 1977].

Stress drop data for transform earthquakes are more limited. Kanamori and Stewart [1976] estimated the fault lengths l for the 1967 and 1974 Gibbs transform events to be 60 and 80 km, respectively, from wave form analysis of body wave phases. When a fault width of 5-10 km is assumed, the possible range of stress drops for both earthquakes is between 30 and 140 bars. Udias [1971] calculated l from the directivity of surface waves and estimated $\Delta\sigma$, assuming $w = l/3$, to be 10-20 bars for two transform events in the North Atlantic.

Fault length can be estimated, in principle, from either the distribution of aftershocks or the corner frequency of the P or S wave amplitude spectral density [e.g., Aki, 1967]. Of the events in Table 2, only the October 16, 1974, Gibbs transform earthquake [Kanamori and Stewart, 1976] had more than two teleseismically located aftershocks. SH corner frequencies f_0 for the six South Pacific and southwest Indian Ocean earth-

TABLE 1. Oceanic Transforms Used in This Study

Transform Code*		Approximate Location	L, km	V, cm/yr	W ₁ , † km	W ₂ , ‡ km	Name
Pole	Number						
	1	52°N, 33°W	280	2.48	4.5	1.5	Gibbs
	1	66°N, 19°W	130	1.99	13.7	1.0	Tjörnes
	2	24°N, 46°W	130	3.17	15.2	0.9	Kane
	2	30°N, 42°W	70	2.95	1.4	0.6	Atlantis
	2	35°N, 36°W	140	2.74	2.0	1.0	Oceanographer
	3	44°N, 128°W	350	5.50	1.7	1.1	Blanco
	3	49°N, 129°W	160	5.28	3.0	0.8	Sovanco
	4	3°S, 105°W	80	16.07	0.3	0.3	
	4	4°S, 102°W	80	16.17	0.6	0.3	
	4	5°S, 106°W	150	16.32	0.4	0.4	
	4	9°S, 109°W	120	16.96	0.4	0.3	
	4	13°S, 92°W	80	17.17	0.2	0.2	
	4	28°S, 113°W	200	18.22	0.3	0.4	
	4	30°S, 112°W	180	18.24	0.2	0.4	
	5	2°N, 91°W	200	5.93	0.9	0.8	
	5	1°N, 85°W	150	6.50	0.4	0.6	
	6	7°S, 68°E	180	3.73	0.4	1.0	
	6	9°S, 69°E	300	3.86	1.4	1.3	
	6	14°S, 68°E	130	4.18	0.4	0.8	
	6	17°S, 66°E	240	4.33	1.1	1.1	
	6	19°S, 66°E	110	4.50	0.4	0.7	
	7	37°S, 78°E	300	6.82	0.6	0.9	
	7	41°S, 80°E	240	7.01	1.0	0.8	
	7	45°S, 87°E	210	7.20	0.8	0.7	
	7	48°S, 98°E	240	7.46	2.5	0.8	
	7	51°S, 140°E	290	7.06	1.1	0.9	
	7	52°S, 141°E	200	7.03	0.5	0.7	
	7	56°S, 146°E	460	6.93	1.5	1.1	
	7	60°S, 149°E	260	6.90	1.4	0.8	
	7	62°N, 154°E	360	6.82	2.7	1.0	
	9	8°N, 104°W	170	12.40	0.5	0.5	
	9	10°N, 104°W	160	11.58	1.0	0.5	
	9	15°N, 105°W	130	9.92	0.2	0.5	
	10	50°S, 115°W	250	9.76	0.4	0.7	Menard
	10	56°S, 123°W	400	8.95	1.5	0.9	Heezen
	10	55°S, 132°W	530	8.84	1.2	1.1	Tharp
	10	57°S, 141°W	370	8.37	0.4	0.9	Udintsev
	10	59°S, 160°W	320	7.28	3.2	0.9	
	10	63°S, 166°W	260	6.56	0.2	0.9	
	11	54°S, 3°W	150	3.69	0.6	0.9	
	11	47°S, 15°W	290	3.91	4.4	1.3	
	11	37°S, 18°W	180	4.04	1.2	1.0	
	11	36°S, 16°W	140	4.05	1.2	0.9	
	11	12°S, 14°W	130	3.84	0.8	0.8	
	11	5°S, 12°W	220	3.70	0.4	1.1	
	11	1°S, 15°W	340	3.56	7.9	1.5	Chain
	11	0°N, 20°W	950	3.48	4.1	2.5	Romanche
	11	1°N, 28°W	610	3.39	2.8	2.0	St. Paul's
	11	7°N, 36°W	510	3.09	16.8	1.9	
	11	8°N, 39°W	140	3.05	9.5	1.0	
	11	11°N, 43°W	330	2.92	41.0	1.6	Vema
	11	13°N, 44°W	80	2.80	1.0	0.7	
	11	15°N, 46°W	180	2.73	1.9	1.2	
	12	56°S, 2°W	220	2.37	14.1	1.3	Conrad
	12	59°S, 12°W	650	2.33	3.6	2.4	
	12	61°S, 20°W	80	2.29	0.6	0.8	
	13	49°S, 32°E	400	1.55	219.3	2.0	
	14	36°S, 98°W	270	7.18	0.7	0.8	
	14	36°S, 97°W	160	7.19	0.5	0.6	
	14	41°S, 89°W	280	7.32	0.1	0.9	

*The transform code includes both a pole entry, identifying the plate boundary, and a transform number for that pole.

†W₁ is the width from the method of Brune [1968].

‡W₂ is the mean depth of 100°C nominal isotherm.

quakes in Table 2 with newly determined moments generally lie in the range 0.02–0.05 Hz for all events, mean corner frequencies varying between 0.03 and 0.045 Hz [Burr, 1977]. By using the source theory of Madariaga [1977] for rectangular faults,

$$l = 0.20\beta/f_0 \quad (7)$$

where β is the shear wave velocity (3.5 km/s), the range in mean corner frequencies corresponds to a range in fault lengths of 15–25 km. For fault widths of 5–10 km these values correspond to a 5- to 80-bar stress drop [Burr, 1977].

TABLE 2. Transform Earthquakes With Known Seismic Moments

Date	Location ^a	Transform Code		M_S^b	m_b^a	$M_0, 10^{25}$ dyn cm	$\eta\bar{\sigma}_s$, bars	$\eta\bar{\sigma}_b$, bars
		Pole	Number					
Oct. 16, 1974	52.71°N, 32.00°W	1	1	6.9	5.7	45. ^c	10.4	0.02
Feb. 13, 1967	52.82°N, 34.25°W	1	1	6.5	5.6	34. ^c	3.4	0.02
March 28, 1963	66.29°N, 19.86°W	1	2	7.0 ^d		27.6 ^e	23.9	
May 19, 1963	24.37°N, 45.97°W	2	1	6.4 ^d	6.0 ^b	24.6 ^e		0.21
May 17, 1964	35.35°N, 36.08°W	2	3	5.8 ^d	5.6	1.94 ^f		0.30
Aug. 22, 1963	42.80°N, 126.19°W	3	1	5.7 ^d	5.6 ^b	0.81 ^e		0.71
July 7, 1964	43.41°N, 127.00°W	3	1		5.1	0.04 ^g		0.90
June 14, 1965	44.61°N, 129.59°W	3	1		5.0	0.16 ^g		0.13
May 22, 1966	21.28°N, 108.74°W	3	0		5.2	0.20 ^g		0.31
May 23, 1966	21.34°N, 108.66°W	3	0		5.2	0.31 ^g		0.20
Dec. 6, 1965	18.99°N, 107.12°W	3	0	6.7 ^d	5.7	13.72 ^g	17.0	0.07
Sept. 9, 1969	4.41°S, 105.82°W	4	3	5.3	4.9	0.48 ^h		0.02
Nov. 18, 1970	28.79°S, 112.77°W	4	6	5.8	5.4	1.37 ^h		0.14
Oct. 12, 1964	31.40°S, 110.84°W	4	7	6.2 ^d	5.9	2.40 ^h		1.25
March 7, 1963	26.83°S, 113.54°W	4	0	6.5 ^d		7.64 ^h	15.3	
Nov. 3, 1965	22.34°S, 113.98°W	4	0	6.0 ^d	5.8	1.94 ^h		0.89
Nov. 6, 1965	22.13°S, 113.76°W	4	0	6.2 ^d	5.7	0.96 ^h		1.04
June 26, 1969	2.08°N, 90.52°W	5	1	5.3	5.0	0.60 ^h		0.03
April 6, 1966	45.81°S, 96.06°E	7	4		5.7	3.76 ^h		0.26
Jan. 21, 1967	49.71°S, 114.90°W	10	1		5.4	3.96 ^h		0.05
April 4, 1971	56.27°S, 122.57°W	10	2	6.6	5.7	8.0 ⁱ	20.7	0.12
Aug. 18, 1969	55.97°S, 123.35°W	10	2	6.4	5.3	1.7 ⁱ		0.06
April 3, 1963	52.13°S, 131.47°W	10	2	6.5 ^d	5.8 ^b	1.33 ^h	88.0	1.30
Sept. 9, 1967	54.80°S, 136.00°W	10	3	6.1	5.1	3.4 ⁱ		0.01
Aug. 24, 1970	56.46°S, 142.61°W	10	4	6.4	5.8	4.4 ⁱ		0.39
Dec. 14, 1964	54.17°S, 1.90°W	11	1	6.2 ^d	5.7	7.99 ^h		0.12
Aug. 16, 1965	0.47°S, 19.93°W	11	8	6.4 ^d	6.0	2.76 ^h		1.89
Nov. 15, 1965	0.21°S, 18.65°W	11	8	6.4 ^d	5.7	2.03 ^h		0.49
Aug. 3, 1963	7.48°N, 35.81°W	11	10	6.8 ^j	6.1 ^b	12.2 ^j	27.0	0.74
Nov. 17, 1963	7.78°N, 37.37°W	11	10	6.5 ^j	5.9 ^b	3.83 ^j	30.6	0.79
June 19, 1960	15.34°N, 45.92°W	11	14	5.8	5.5	1.03 ^j		0.32
Nov. 10, 1942	49.40°S, 30.60°E	13	1	7.9 ^k		2800. ^l	5.3	
June 8, 1968	48.94°S, 31.22°E	13	0	6.0	5.6	2.5 ⁱ		0.23
Jan. 8, 1974	38.84°S, 46.43°E	13	0	6.1	5.9	1.8 ⁱ		1.67
April 19, 1974	41.67°S, 84.00°W	14	3	5.9 ^d	5.4	0.94 ^h		0.20
Oct. 6, 1964	36.20°S, 100.92°W	14	1	5.9 ^d	5.2	2.93 ^h		0.02

^aInternational Seismological Summary/International Seismological Centre.

^bU.S. Coast and Geodetic Survey/NOAA/USGS.

^cKanamori and Stewart [1976].

^dRothé [1969].

^eWyss [1970].

^fWeidner and Aki [1973].

^gTsai [1969].

^hForsyth [1973].

ⁱThis study.

^jUdias [1971].

^kGutenberg and Richter [1954].

^lBrune and King [1967], Brune [1968].

RELATIONS AMONG SOURCE PARAMETERS, TRANSFORM GEOMETRY, AND SPREADING VELOCITY

As was noted above, the measure of earthquake size most clearly related to fault dimensions and slip is the seismic moment. The earthquakes in Table 2 represent the full population of transform events with known moment. Because magnitude data for transform earthquakes span a larger population representing a longer sampling time, a rule for converting magnitudes to moments for transform events is desirable to increase the data base for discussion of the factors controlling source properties.

Figure 2 is a plot of M_0 versus M_S for the earthquakes in Table 2. Shown as solid symbols are the events with both a measured moment and a surface wave magnitude reported by the USGS, the two events with M_0 and M_S measured by Udias [1971], and the magnitude 7.9 event from the southwest Indian ridge. Open symbols are for events with published moments and a magnitude given by Rothé [1969]. The M_0 versus M_S curves from the ω^2 and ω^3 models of Aki [1967], as scaled by Brune and King [1967] and Brune [1968], are shown with

dashed lines. The two sets of data show similar trends, but the open symbols display somewhat more scatter. The solid symbols will be used as reference markers for moment-magnitude relations to be derived below.

The relation between M_0 and M_S shown in Figure 2 for Aki's [1967] ω^2 model fits the data shown reasonably well. As this source model provides a good fit to long-period source spectra for other large earthquakes [Aki, 1972], we use this curve below to estimate M_0 for transform earthquakes for which only M_S is available.

The moments of transform earthquakes are related to other transform properties in the following graphs, by using both the population of events with known moments (Table 2) and the population of events with known magnitudes and the moment-magnitude relation of Figure 2. Plots of M_0 versus spreading velocity V are shown in Figures 3 and 4, where M_0 is either measured or estimated from the magnitude, respectively. Figure 5 shows the moment sum versus V for the population of 60 transforms in Table 1.

All three graphs show the feature that the maximum mo-

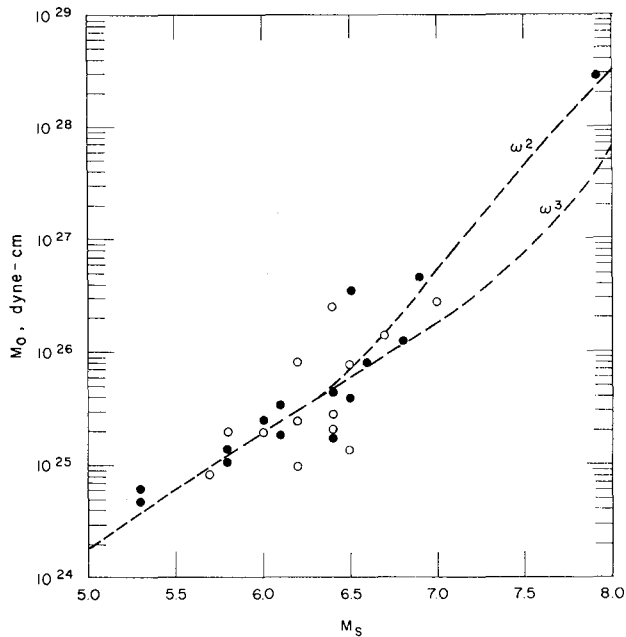


Fig. 2. Plot of M_0 versus M_s for all earthquakes in Table 2. Solid symbols are those with M_s from the USGS or *Udias* [1971] and the $M = 7.9$ event [Gutenberg and Richter, 1954] on the southwest Indian ridge. Open symbols are those with magnitudes from *Rothé* [1969]. Dashed lines are from the ω^2 and ω^3 models of *Aki* [1967] as scaled by *Brune and King* [1967] and *Brune* [1968].

ment on a transform tends to decrease as spreading rate increases. This trend is best displayed by the larger data sets (Figures 4 and 5).

Figures 6, 7, and 8 show the relation between M_0 or $\sum M_0$ and transform length for the same data sets. On all three figures the upper bound on M_0 or $\sum M_0$ appears to increase as the transform length increases for lengths less than 400 km, though this trend is produced by only a few key points on each

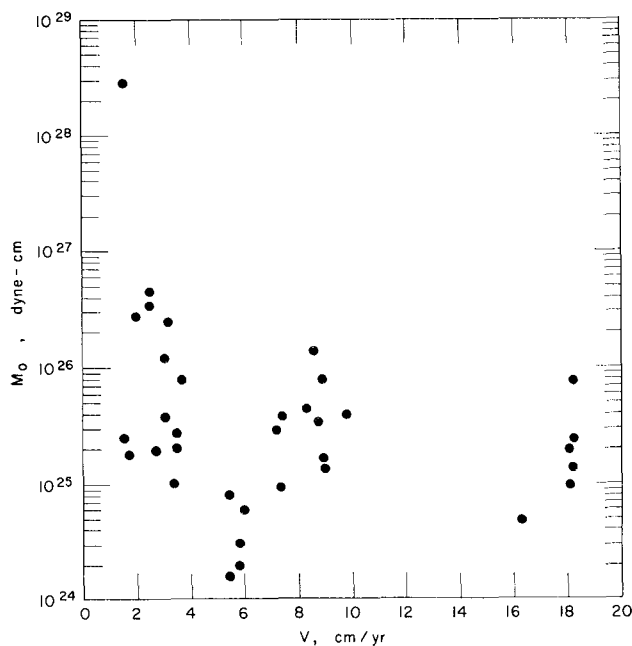


Fig. 3. Plot of M_0 versus spreading rate V for earthquakes in Table 2.

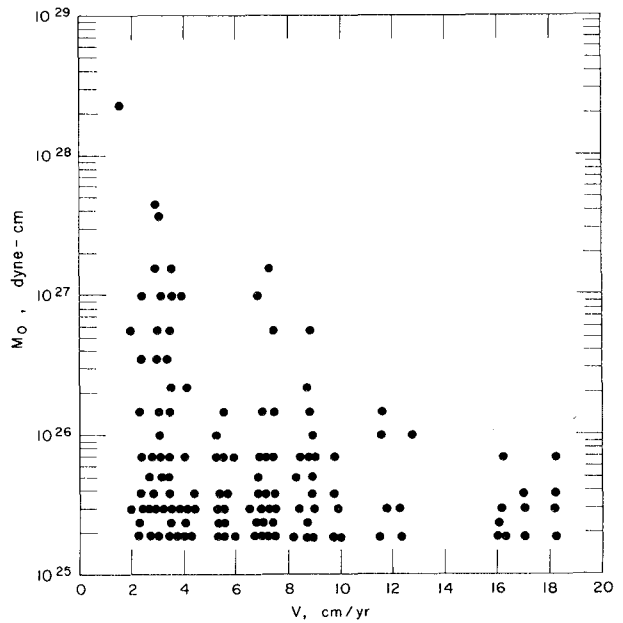


Fig. 4. Plot of M_0 versus spreading rate V using earthquakes with known magnitudes and the moment-magnitude relation given by the ω^2 model in Figure 2.

graph. Above 400-km length there may be a decrease in maximum moment with increasing length. Since the magnitude 7.9 event may represent a break of the entire transform of such a length on a very slow spreading ridge, the apparent maximum may represent a mechanical inability to break completely a substantially longer fracture zone (e.g., Romanche, 950 km long) coupled with higher V (and thus higher temperatures) on the other long transforms. In Figure 6 are two earthquakes (the third and fourth entries in Table 2) with large moments [Wyss, 1970] on relatively short (130 km) transforms, Kane

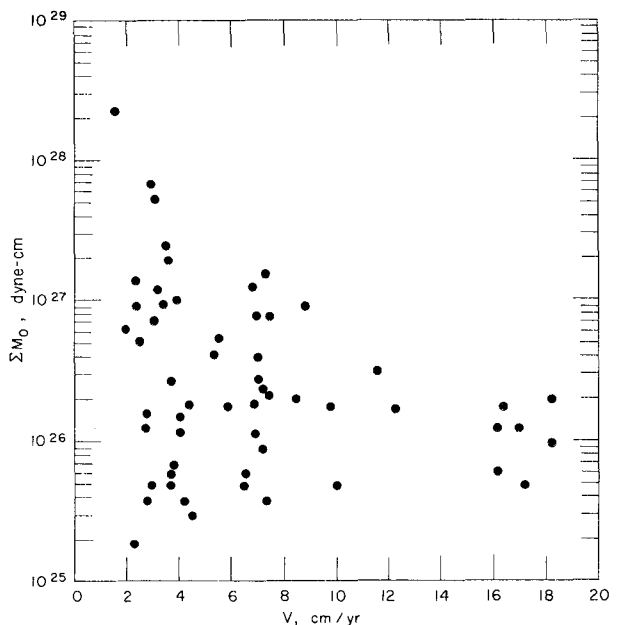


Fig. 5. Plot of moment sum versus spreading for each transform using all known earthquake magnitudes and the moment-magnitude relation given by the ω^2 model in Figure 2.

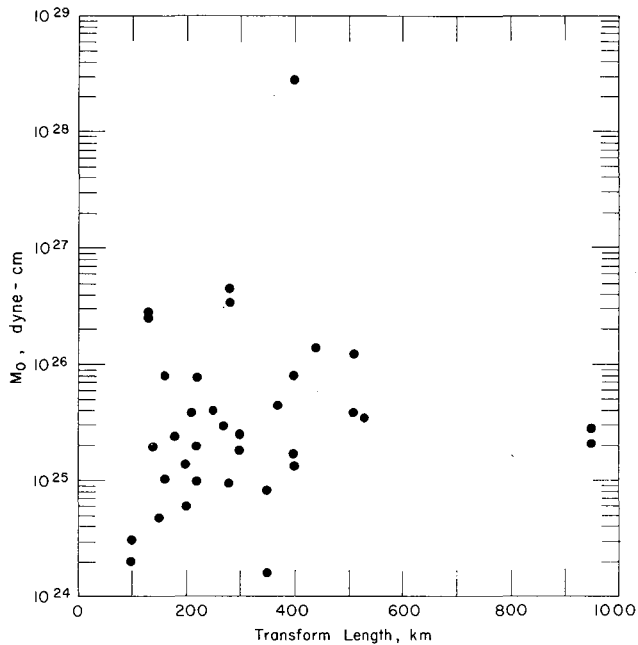


Fig. 6. Plot of M_0 versus transform length for the earthquakes in Table 2.

and Tjörnes. (The two symbols almost superpose in the figure.) These events may also represent breakage of the entire transform. Because the Tjörnes transform is an unusually complex zone of deformation, 75 km in width and composed of several troughs and apparent volcanic chains nearly orthogonal to the transform strike [Saemundsson, 1974], the 1963 $M_s = 7.0$ earthquake may have involved a larger source volume than is typical of transforms of that length.

A second trend apparent in Figure 8 is for the minimum $\sum M_0$ to increase as transform length increases. This trend and the two relations noted above for maximum M_0 versus L and

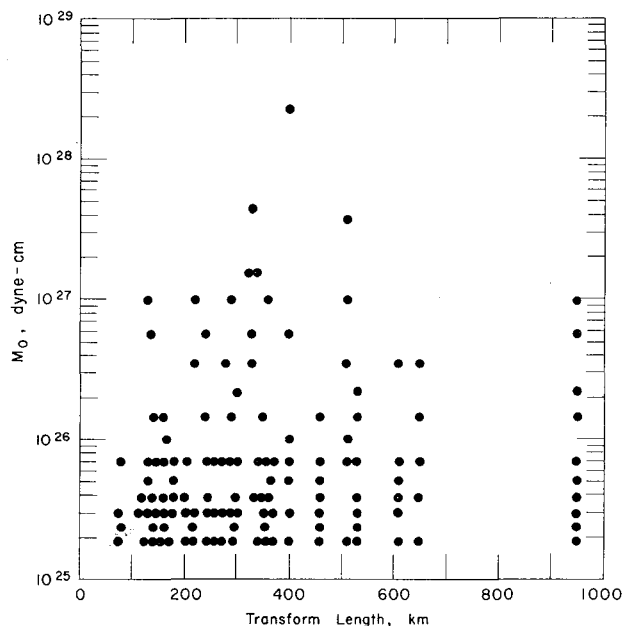


Fig. 7. Plot of M_0 versus transform length using earthquakes with known magnitudes and the moment-magnitude relation given by the ω^2 model in Figure 2.

V indicate that both slip rate and fault length are controlling faulting in some fashion on these oceanic transforms.

Another important parameter is the transform width. One can solve for W from (2) [Brune, 1968]

$$W = \sum M_0 / \mu L V T \quad (8)$$

Adopting a value for T (sample time) is not straightforward because transforms may be inactive for substantial periods of time and because some earthquakes above magnitude 6.0 may not have been reported. A value of 50 years seems to allow for both problems on most transforms, but there may be an error as large as 15 years for some. The rigidity μ is taken to be 3.3×10^{11} dyn/cm². An average width has been calculated for each transform by this method, and these widths are compiled in Table 1. The important considerations to keep in mind when one is using the above formula are that (1) all movement on the fault is assumed to be brittle failure and (2) owing to the nature of the M_0 versus M_s and M_s versus frequency curves, earthquakes smaller than $M_s = 6.0$ will not contribute significantly to the moment sum. If likely errors are taken into consideration, W is generally good to a factor of perhaps 2–3 but may be greatly overestimated if the earthquake population contains a rare large event. For comparison, Brune [1968] estimated $W = 6.5$ km for the combined Chain, Romanche, and St. Paul's transforms, 1.2 km for the Eltanin system (Heezen and Tharp transforms), and 3.1 for the vicinity of the Jan Mayen transform.

Figure 9 shows a plot of W versus transform length. Common symbols represent the trend of transforms having approximately the same slip rate. There is a tendency for width to increase as transform length increases for transforms of similar velocity, except perhaps at the highest slip rates.

To explain this observation, and ultimately the trends noted in earlier figures as well, it is necessary to look at the thermal structure along the transform (Figure 1). At the ridge crest, hot material is added to one side of the transform, and as this material moves away from the ridge axis, it cools and con-

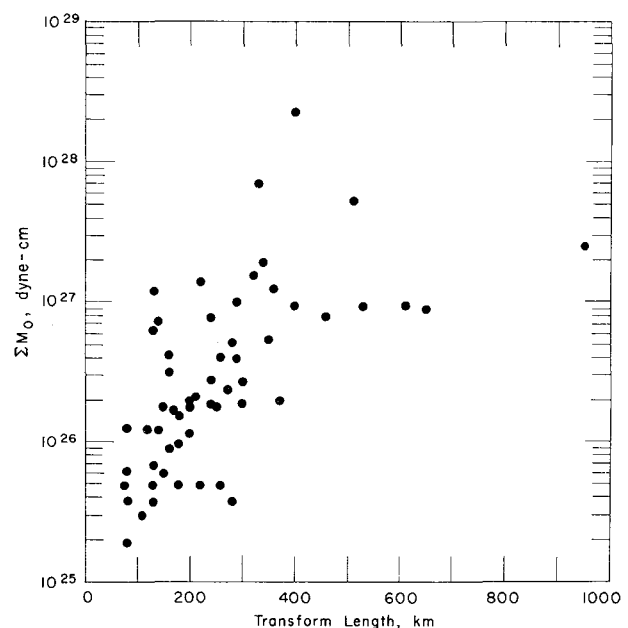


Fig. 8. Plot of moment sum versus transform length for each transform using all known earthquake magnitudes and the moment-magnitude relation given by the ω^2 model in Figure 2.

tracts. Rocks at high temperature will tend to flow rather than fracture, so one would expect that very near the ridge crest, where the crust is very hot, brittle failure may occur only very near the surface. As the crust cools and moves away from the ridge, brittle failure will occur deeper in the crust.

Consider the fact that along faster transforms the isotherms in the crust are closer to the surface than along slower ones. Also notice in Figure 9 that the slower transforms get wider more quickly as length increases. From these two observations we postulate that the area of brittle failure is controlled by the depth to a certain isotherm. We explore this idea further in the next section.

Figure 10 shows the relationship between W and V . Note a large decrease in the maximum computed width as spreading rate increases. (For clarity, the graph shows only widths less than 8 km. There are also some larger apparent widths on transforms with velocities less than 3.0 cm/yr; see Table 1). This graph can be partially explained by the thermal structure as discussed above for Figure 10, but another factor is also causing this relation, as is shown in Figure 11.

Figure 11, a plot of transform length versus spreading rate, shows that maximum length decreases as spreading rate increases. The cause of the relation may involve many diverse factors. First, the pattern may be merely a coincidence that will change with time. Such a 'coincidence' as this must have held, however, for at least the last 100 m.y. because the 950 km-long Romanche fracture zone has been in existence that long and the mid-Atlantic ridge has had about the same spreading rate relative to other ridges as it does now. Most of the major transforms can be traced back to continental margin offsets via fracture zones. Thus it is the original pattern by which continents break apart that determines where many of the large transforms will occur. That the east Pacific rise has mainly small fracture zones may be due to the fact that this ridge has not represented the junction between two continents for the last few hundred million years, if ever.

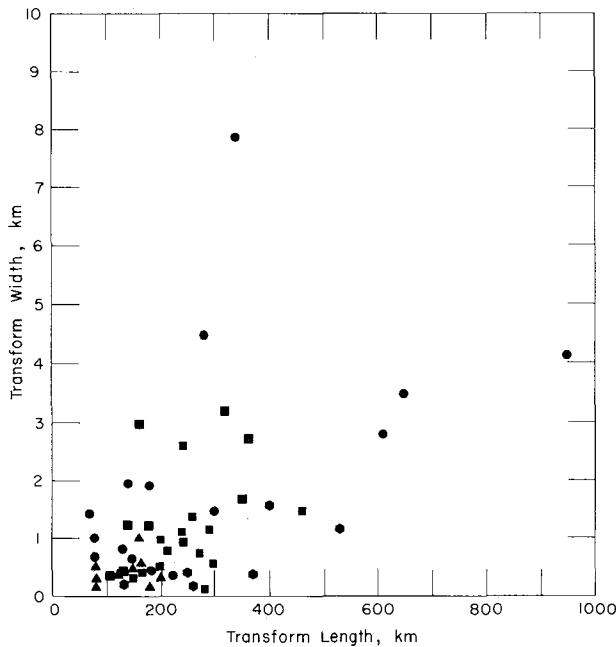


Fig. 9. Plot of effective transform width W versus transform length L . Symbols show trends of transforms with similar spreading rates (circles, $V = 0-4$ cm/yr; squares, $V = 4-7.5$ cm/yr; hexagons, $V = 7.5-11$ cm/yr; and triangles, $V = 11-18$ cm/yr).

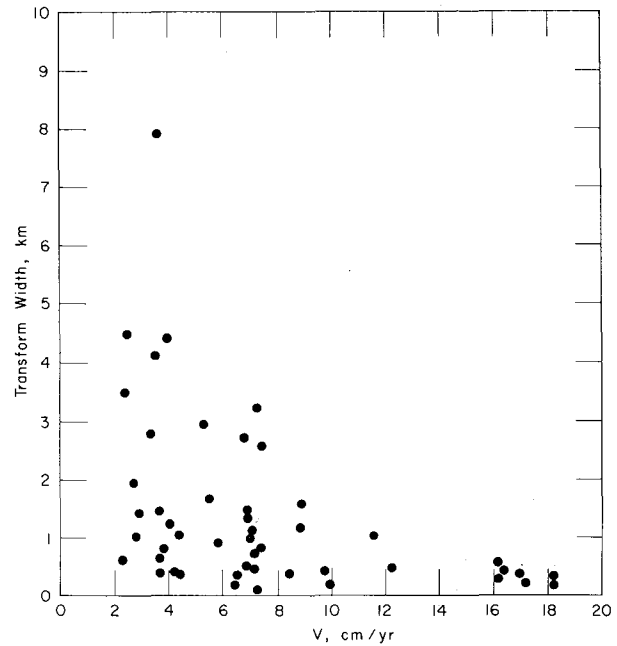


Fig. 10. Plot of effective transform width W versus spreading rate V .

One phenomenon that might break up a transform is relative motion between the transform and the pole of rotation for the two adjoining plates. This motion would tend to put the transform under either compression or extension. Extension would form a spreading center within the transform (e.g., a 'leaky' transform), and compression would shorten or deform the transform and might lead to ridge jumps or asymmetric spreading. In the right circumstances, asymmetric spreading, or a ridge jump, could also lengthen a transform. All of the above effects would be felt most heavily on a transform with a fast slip rate due to its hotter, weaker lithosphere. It is possible that the least energy configuration of a ridge would be many small transforms as opposed to a few large ones, but such a point is debatable. Perhaps long fracture zones inhibit changes in spreading poles by their inability to change shape and restrict spreading rate by frictional resistance.

Apparent stress was plotted against all the other parameters (V , L , and W), but no clear relation could be discerned. Thus from the available data it does not appear that spreading rate

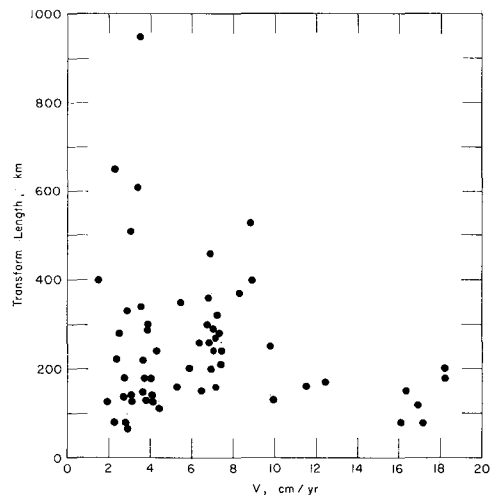


Fig. 11. Plot of transform length L versus slip rate V .

or transform length has a noticeable effect on the magnitude of the lithospheric stress field around oceanic transforms.

THE INVERSE PROBLEM

In the previous section a moment-magnitude relation was used to assign moments to earthquakes so that information about the fault width could be ascertained. If this is considered the forward problem, then a corresponding inverse problem is to take the width as known from independent information and invert the earthquake data to obtain a moment-magnitude curve. The depth to a specified isotherm within a transform, as was suggested in the last section, is assumed to be the independent parameter from which fault width may be determined.

Ideally, what is needed is the thermal structure of each oceanic transform. Unfortunately, the shallow thermal structure of transforms has never been modeled in detail, and until the geology and the factors controlling topographic features within the slip zone are known, such structure will be difficult to estimate reliably. The thermal structure of normal oceanic lithosphere, however, is reasonably well understood from spreading plate thermal models [e.g., *Sleep, 1975*]. Such thermal models have been shown to have predictive value for modeling the seismic velocity and Q structure of oceanic lithosphere and asthenosphere [*Forsyth and Press, 1971*; *Solomon, 1973*; *Solomon and Julian, 1974*; *Duschenes and Solomon, 1977*] and the mechanical properties of ridge axes [*Solomon, 1976*]. It will be assumed that the temperature from the spreading plate model holds for each side of a transform as well.

According to spreading plate thermal models a given isotherm is closer to the surface on the side of the fault closest to the spreading center (Figure 1). It is only in the center that a given isotherm is at the same depth on both sides of the fault. If a single isotherm limits brittle behavior, then there are two

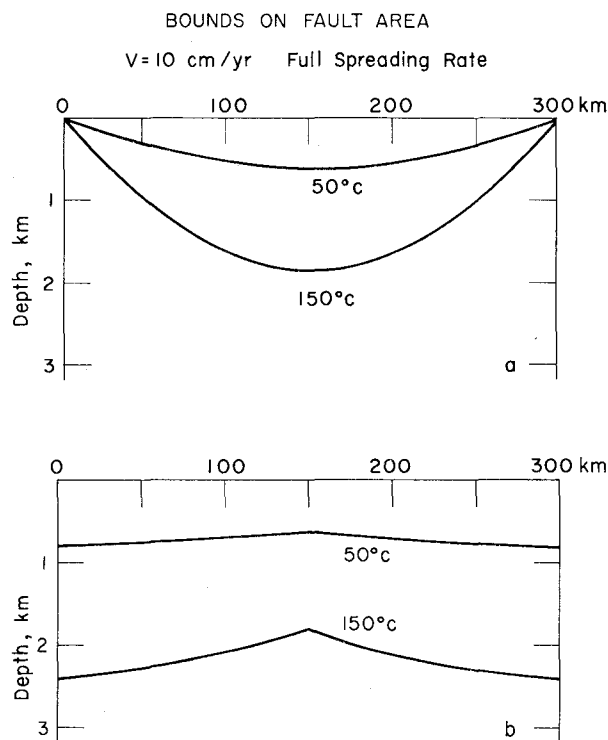


Fig. 12. Possible bounds on the area of a transform undergoing brittle failure for $L = 300$ km and $V = 10$ cm/yr [*Sleep, 1975*]. (a) Minimum depth to isotherm shown. (b) Maximum depth to isotherm shown.

simple bounds on the shape of the faulting area, as shown in Figure 12. The first area represents the shallowest depth to a given isotherm, and the second represents the greatest depth to a given isotherm.

To pose the inverse problem we first write the equation for the predicted moment sum s_i for the i th transform from the fault slip theory of *Brune* [1968]:

$$s_i = \mu L_i W_i V_i T_i \quad (9)$$

where L_i , W_i , V_i , and T_i are the transform length, width, slip rate, and sample time, respectively. The quantities L_i , V_i , and T_i are all known. The width W_i can be calculated for a given isotherm once a rule for determining isotherm depth is specified (e.g., Figure 12a or 12b). From the known earthquakes on the i th transform, the moment sum $\sum M_0$ from seismic magnitude observations is

$$\sum M_0 = \sum_{j=1}^{18} a_{ij} c_j \quad (10)$$

where a_{ij} is the number of earthquakes of the j th magnitude on the i th transform and c_j is the moment corresponding to the j th magnitude, according to the moment-magnitude relation to be determined.

The matrix A of magnitude data used in the inversion is given in Table 3. Note that in this study only the thirteen discrete magnitudes 6.0, 6.1, 6.2, \dots , 7.2 are used. The three transforms in Table 1 with events larger than 7.2 (11-10, 11-12 Vema, and 13-1) are not included because too few events of such magnitude have occurred to perform meaningful inversion.

Equating the right-hand sides of (9) and (10) and solving for the c_j will give a moment-magnitude relation that can be compared, for each adopted isotherm, to the data of Table 1 and Figure 2. If the trends are the same, it will confirm the hypothesis that the depth to a certain isotherm is the controlling parameter for fault area. The position of the resultant curve will be determined by the limiting temperature picked to calculate the fault widths. Thus matching the position of the curve to the data in Figure 2 will give at least a nominal value to the temperature controlling the depth of brittle failure.

The combination of (9) and (10) results in the matrix equation

$$S = AC \quad (11)$$

which is an overdetermined set of linear equations. Premultiplying (11) by A^T (the transpose of A) gives a system of linear equations,

$$A^T S = A^T A C \quad (12)$$

where $A^T A$ is a square, nonsingular, symmetric matrix. The solution vector C can be found by using standard routines for solving a system of linear equations.

Since the relation log moment versus magnitude can be approximated by a straight line, at least for magnitudes less than about 7.0, it is convenient to do a linear least squares fit of the log of the vector C as a function of the respective magnitudes. This gives a slope and a position to a line which is easily compared to other log moment-magnitude relations. The discrete solution C is useful, in some respects, because it indicates how well the moment for each magnitude is determined. However, the discrete solution is not as important as the least squares solution because the magnitudes for most of the early earthquakes used [*Gutenberg and Richter, 1954*] are

TABLE 3. Matrix *A* of Magnitude Data by Transform

Transform Code	Num- Pole	<i>M</i>												
		6.0	6.1	6.2	6.3	6.4	6.5	6.6	6.7	6.8	6.9	7.0	7.1	7.2
1	1	0	0	1	0	0	2	0	0	0	1	0	0	0
1	2	0	0	2	0	0	0	0	0	0	0	1	0	0
2	1	0	0	1	0	1	2	0	0	0	0	0	1	0
2	2	1	0	1	0	0	0	0	0	0	0	0	0	0
2	3	3	0	1	1	0	0	0	0	0	0	0	0	0
3	1	5	1	2	2	0	2	0	1	0	0	0	0	0
3	2	3	1	2	1	0	2	1	0	0	0	0	0	0
4	1	2	1	0	0	0	0	0	0	0	0	0	0	0
4	2	0	1	1	0	0	1	0	0	0	0	0	0	0
4	3	2	0	0	0	0	2	0	0	0	0	0	0	0
4	4	3	0	1	1	0	0	0	0	0	0	0	0	0
4	5	1	0	1	0	0	0	0	0	0	0	0	0	0
4	6	2	0	3	0	0	1	0	0	0	0	0	0	0
4	7	1	0	0	2	0	0	0	0	0	0	0	0	0
5	1	2	0	0	0	0	2	0	0	0	0	0	0	0
5	2	0	0	2	0	0	0	0	0	0	0	0	0	0
6	1	1	0	1	0	0	0	0	0	0	0	0	0	0
6	2	1	0	1	0	0	0	0	1	0	0	0	0	0
6	3	2	0	0	0	0	0	0	0	0	0	0	0	0
6	4	3	0	3	1	0	0	0	0	0	0	0	0	0
6	5	0	0	1	0	0	0	0	0	0	0	0	0	0
7	1	3	1	0	1	0	1	0	0	0	0	0	0	0
7	2	0	0	2	0	0	1	0	1	0	0	0	0	0
7	3	1	1	1	0	0	2	0	0	0	0	0	0	0
7	4	1	0	0	1	0	0	0	1	0	0	1	0	0
7	5	2	2	3	0	0	1	0	1	0	0	0	0	0
7	6	4	0	0	1	0	0	0	0	0	0	0	0	0
7	7	5	1	6	3	3	1	0	1	0	0	0	0	0
7	8	2	0	3	0	0	4	0	0	0	0	0	0	0
7	9	1	1	1	2	1	1	0	0	0	0	0	1	0
9	1	2	0	1	0	0	0	1	0	0	0	0	0	0
9	2	2	0	1	0	0	0	1	1	0	0	0	0	0
9	3	1	0	1	0	0	0	0	0	0	0	0	0	0
10	1	2	0	1	1	0	1	0	0	0	0	0	0	0
10	2	1	0	2	0	1	2	1	0	0	0	1	0	0
10	3	5	2	2	2	0	4	0	1	1	0	0	0	0
10	4	1	0	2	0	1	1	0	0	0	0	0	0	0
10	5	0	0	0	0	0	0	0	0	0	0	0	0	1
10	6	1	0	1	0	0	0	0	0	0	0	0	0	0
11	1	0	0	2	0	0	0	0	0	0	0	0	0	0
11	2	1	0	0	0	0	0	0	0	0	0	0	1	0
11	3	1	0	2	0	0	1	0	0	0	0	0	0	0
11	4	0	2	0	0	0	1	0	0	0	0	0	0	0
11	5	2	0	1	0	0	0	0	0	0	0	0	0	0
11	6	1	0	1	0	0	0	0	0	0	0	0	0	0
11	7	2	0	0	1	0	4	0	0	0	0	0	0	1
11	8	3	2	6	1	2	2	0	1	1	0	1	1	0
11	9	4	0	3	3	1	4	0	0	0	1	0	0	0
11	11	0	0	0	0	0	0	0	1	0	0	1	0	0
11	13	2	0	0	0	0	0	0	0	0	0	0	0	0
11	14	2	0	0	0	1	1	0	0	0	0	0	0	0
12	1	0	1	1	0	0	0	0	0	0	1	0	1	0
12	2	1	0	0	1	0	3	0	2	0	1	0	0	0
12	3	1	0	0	0	0	0	0	0	0	0	0	0	0
14	1	2	0	2	0	0	2	0	0	0	0	0	0	0
14	2	1	0	0	0	0	1	0	0	0	0	0	0	0
14	3	2	0	0	0	0	0	0	0	0	0	0	0	0

typically given only to the nearest quarter, rather than tenth, of a magnitude unit.

Figure 13 shows the results of the inversion of the data from the 57 transforms in Table 3 using four different temperatures to determine the fault areas (Figure 12a). When the least squares lines are compared with the data from Figure 2, it is evident that the isotherm that best matches the moment-magnitude data is about 150°C.

The discrete moment-magnitude solution for the above 57 transforms, given in Figure 14, shows that each $M_0(M_s)$ is not very well defined. The data set has a positive slope for each isotherm, however. Much of the jaggedness of Figure 14 is due to inclusion of several transforms in Table 3 which seem to have an abnormally large or small number of earthquakes for their length and velocity. This sampling problem is reflected in the calculation of anomalous widths for those transforms

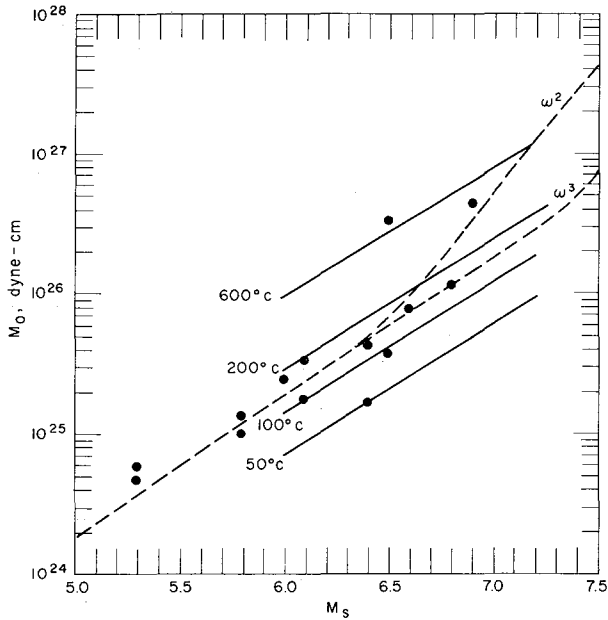


Fig. 13. Predicted log moment versus magnitude relations based on a least squares linear representation of the results of inversion of slip rate and magnitude data from 57 transforms. Each line represents a different isotherm used to determine the transform area as in Figure 12a. Data are the solid symbols from Figure 2.

(Table 1), which include 1-2 (Tjörnes), 2-1 (Kane), 3-1 (Blanco), 3-2 (Sovanco), 7-1, 10-6, 12-1 (Conrad), and 14-3.

The discrete solution for the remaining 49 transforms (Figure 15) has a much smoother solution for $M_0(M_S)$. In the least squares sense (Figure 16) the slopes remain the same as the previous solution (Figure 13), but the position of each line is moved up slightly. By using the 100°C isotherm, which is the best fit for this case, an average width has been computed by dividing the area above the isotherm for each transform by the transform length. These widths have been compiled in Table 1.

The eleven anomalous transforms may have a non-representative sample of earthquakes or may be affected by some other phenomenon (e.g., compressive stress) more severely than are the others.

The slopes of the lines in Figures 13 and 16 are very close to the prediction of the ω^3 model, perhaps indicating support for the model. The data from Figure 2, however, indicate that the moment-magnitude relation is best described by a curve intermediate between the ω^2 and ω^3 models. This apparent discrepancy may be due to the least squares solution smoothing out any trend for a slope increase at higher magnitudes, but such a trend is not apparent in the discrete solutions, and one would expect, in such a case, a slope slightly larger than that for the ω^3 curve. The apparent discrepancy may also be due to a magnitude dependence for the controlling isotherm for large magnitude transform events. We elaborate on this possibility below.

There are many factors which introduce uncertainties in the estimate of the best fitting isotherm that limits the depth of seismic failure. The time period over which earthquakes have been included may not have been a fair representative of long-term activity. A small contribution to the net slip from $M < 6$ earthquakes has been ignored. Along portions of some transforms, shear stresses may be partially or completely relieved by aseismic creep, as has been documented for the central San Andreas [Savage and Burford, 1971]. Creep might be expected along portions of the transform with abundant serpentine, for instance. Also, layer 2A in the oceanic crust may have little strength, a possibility which would cause the estimate of temperature to be too low. The area enclosed by the ocean floor and the smallest depth to an isotherm (Figure 12a) may underestimate the area that is cooler than the given temperature; when the geometry in Figure 12b is assumed, the best fitting isotherm drops to 75°C (Figure 17). Some long transforms may have short, yet undiscovered, spreading center segments within them.

It must be emphasized that the temperatures discussed above and shown in Figures 12-17 are nominal temperatures

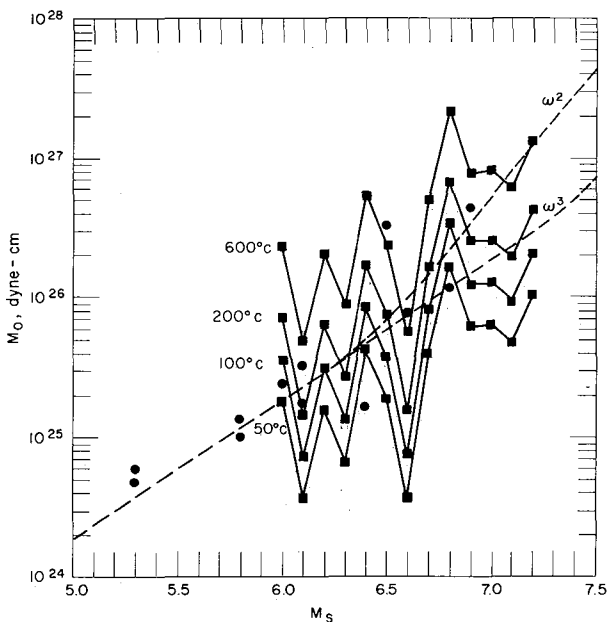


Fig. 14. Discrete solution $M_0(M_S)$ for 57 transforms and 4 isotherms. The transform area is as defined in Figure 12a. Data are from Figure 2.

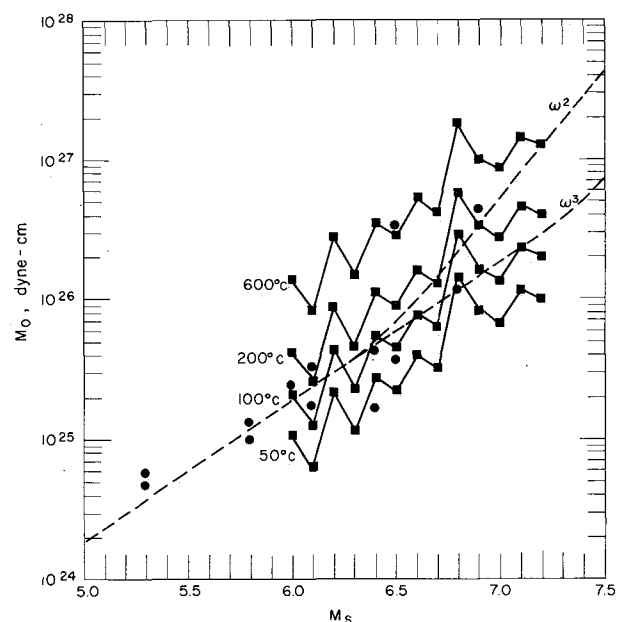


Fig. 15. Discrete solution $M_0(M_S)$ for 49 selected transforms and 4 isotherms (see text). The transform area is as defined in Figure 12a. Data are from Figure 2.

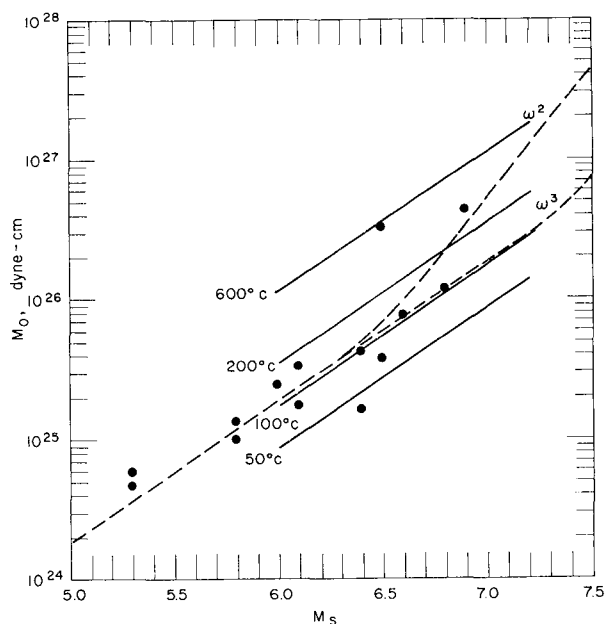


Fig. 16. Least squares representation of the discrete solutions for 49 transforms and 4 isotherms from Figure 15.

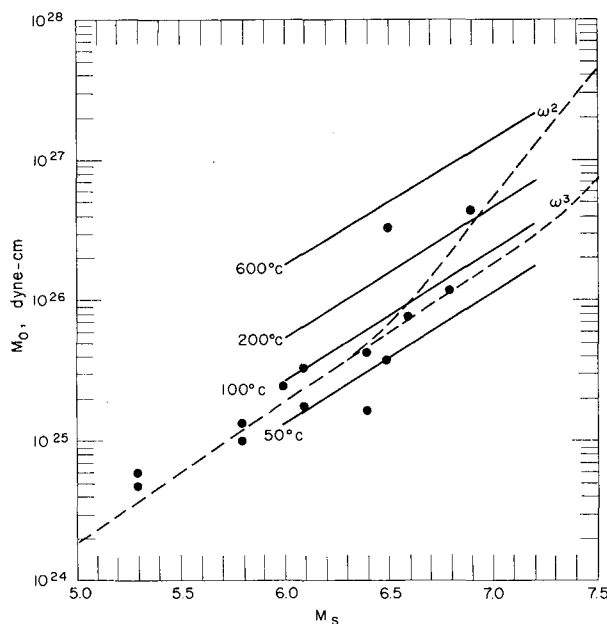


Fig. 17. Least squares representation of the solution $M_0(M_s)$ for 57 transforms using a transform area as defined in Figure 12b. Data are from Figure 2.

only, based on the idealized spreading plate thermal model. Several complexities are likely in actual transform structures. (1) Lateral heat conduction across the fault will tend to average the temperatures on the two sides. (2) The marked topography across most transforms, particularly the characteristic linear trough several hundred meters to several kilometers below the normal ocean floor depth, will complicate the shallow thermal structure. (3) The transform material may be physically or chemically distinct from normal oceanic crust and mantle, thus altering the heat conduction properties. (4) Hydrothermal circulation may be an important heat transfer mechanism in the fault zone. (5) Shear heating may be a significant heat source along the fault. (6) Some transforms may 'leak' in response to regional extension or to a change in rotation pole, raising the temperatures in the shear zone and presumably decreasing the fault width. Meridional extension has been suggested for regions of the North Atlantic [Collette et al., 1974], but the transform widths are, if anything, larger than the norm rather than smaller in that area.

Finally, it should be mentioned that the average fault widths and the nominal temperatures limiting seismic failure are predicated on the simple model of rectangular faults with uniform fault displacements. On an actual fault the slip varies with position and, in particular, decays with depth below the level of maximum slip. Thus some seismic slip almost certainly occurs at depths greater than the fault and transform widths calculated here.

One observation that helps to resolve at least the shape of the transform area generally undergoing seismic failure is the location on the transforms where large earthquakes occur. Though the locations of earthquakes are not always precise enough to determine exactly where they occur in relation to the ridge crests, as a general rule the largest earthquakes on a transform are located toward the transform centers. A good illustration of this observation is the map in Figure 18 of the Romanche fracture zone. The events with $M \geq 6.5$ are all at least 200 km from the ridge axes, and the largest earthquake occurred near the transform center. The major reason for this

pattern is likely the increase in fault width away from the ridge crests, which permits the occurrence of larger magnitude events. The pattern cannot be generally explained as being due to large events rupturing a distance all the way to the ridge crest except in rare instances of very large events and transforms shorter than the Romanche.

DISCUSSION AND CONCLUSIONS

In this study of earthquakes occurring on oceanic transforms we have noted the following relationships. (1) The maximum moment, average fault width, and maximum moment sum all decrease with increased spreading rate. (2) The maximum moment and maximum moment sum appear to increase with transform length up to a length of 400 km and may decrease or may conceivably continue to increase with length for longer transforms. (3) Minimum moment sum and average width also increase with transform length. (4) Larger earthquakes generally occur toward the center of a transform.

From these observations the hypothesis was formulated that an isotherm in the transform zone controls the lower limit of the area over which brittle failure occurs. An inversion of magnitude and slip rate data supports this hypothesis and gives a range of nominal temperatures that could be controlling faulting of between 75°C and 150°C. Uncertainties in

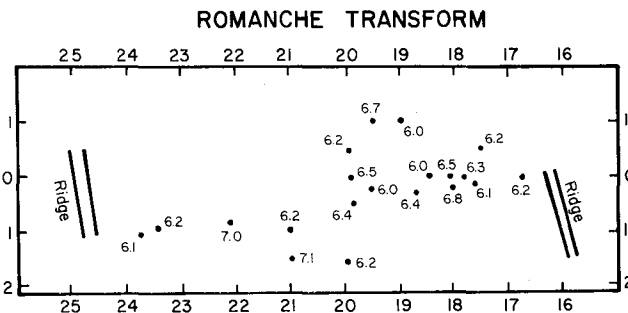


Fig. 18. Earthquakes of magnitude 6.0 and greater occurring on the Romanche transform during the period 1920-1975.

the shape and depth of the isotherms within the transform widen this range considerably. More reasonable bounds on the actual value of the limiting isotherm are probably 50°C and 300°C.

The average fault widths implied by the inversion results are 1 km or less for the shorter transforms and a few kilometers for the longer transforms (Table 1). These fault widths are consistent with available seismic evidence restricting hypocentral depths of transform earthquakes to values of a few kilometers. Tsai [1969] determined focal depths of 4–5 km for about a dozen oceanic transform earthquakes from the amplitude radiation patterns of surface waves. Weidner and Aki [1973] determined focal depths of 6 ± 3 km for two Atlantic transform events from Rayleigh wave phase and amplitude spectra. Sonobuoy and ocean bottom seismometer observations limit the focal depth of transform aftershocks in the Gulf of California to 3–5 km [Reichle *et al.*, 1976] and of microearthquakes on the Rivera fracture zone to less than 10 km [Prothero *et al.*, 1976].

Are the limiting temperatures suggested by the inversion results reasonable boundaries separating seismic from aseismic stress release? Several investigators [Brace and Byerlee, 1970; Stesky *et al.*, 1974] have looked at the transition between stick slip and stable sliding on faults in natural rock samples. They have concluded that this boundary is dependent on temperature, pressure, and composition of the faulting material. At 4-kbar pressure, Stesky *et al.* [1974] found that San Marcos gabbro and Twin Sisters dunite are characterized by stable sliding at temperatures above 150°–200°C and that Mt. Albert peridotite started stable sliding at a transition temperature well below 100°C. Thus the temperatures from the inversion correspond to those obtained in laboratory investigations on rocks which are representative candidates for the material being faulted in the transform.

The hypothesis of an isotherm limiting the depth of seismic failure on oceanic transforms is therefore consistent with the earthquake magnitude data set in Table 3, the known focal depth of transform earthquakes, and laboratory data on the transition from stick slip to stable sliding on rocks likely to be similar in composition to those in the transform zone. The single limiting isotherm model does not account, however, for the rare transform events of very large magnitude and moment or for the occasional anomalous transform with too many $M > 6$ earthquakes for its length and predicted slip rate.

It appears likely that large transform earthquakes ($M \geq 7$) are associated with faulting to greater depth than smaller events. One explanation is that a hotter limiting isotherm is involved for the large magnitude events, perhaps owing to a similarity of the local geotherm to the temperature-pressure curve bounding stick slip and stable sliding behavior [e.g., Stesky *et al.*, 1974]. A second possibility is that the few transforms with very large events have atypically cool thermal structure, perhaps due to enhanced hydrothermal circulation. A third explanation might be predicated on the model for transform fault dynamics [Thatcher, 1975] calling for loading along the base of the fault by aseismic creep of the underlying material. This model would suggest that the fault depth is limited by the ability of material to creep far enough to precipitate the seismic slip. It is possible that for larger magnitude events a large amount of creep is needed, so that only that material at a higher temperature can creep the required distance. This may be in contrast to lower magnitude events, which might require only a small amount of creep that can be accomplished by shallower, lower-temperature material.

Thus while this study has synthesized a large number of data into a simple thermal/mechanical picture of oceanic transforms, the need for further work is clear. Detailed study of the source mechanisms of very large transform events will be fruitful. Further modeling of the thermal structure of transforms is needed so that a more accurate determination of the role of temperature in controlling the fault width can be defined. The moment-magnitude curve needs more data for $M > 7$ transform earthquakes so that a discrimination can be made between various source models. Finally, the analysis of additional source spectra may lead to a determination of relations among stress drop, apparent stress, slip rate, and transform length which have been left unresolved by the present work.

Acknowledgments. We thank Bill Ellsworth, Mike Fehler, Randy Richardson, Steve Taylor, and George Zandt both for advice and for several stimulating discussions. Norm Sleep offered several helpful suggestions on the manuscript. This research was supported by the Division of Earth Sciences, National Science Foundation under NSF grants EAR75-14812 and EAR77-09965 and by the Advanced Research Projects Agency and was monitored by the Air Force Office of Scientific Research under contract F44620-75-C-0064.

REFERENCES

- Aki, K., Generation and propagation of G waves from the Niigata earthquake of June 16, 1964, 2, Estimation of earthquake moment, released energy, and stress-strain drop from G wave spectrum, *Bull. Earthquake Res. Inst. Tokyo Univ.*, **44**, 73–88, 1966.
- Aki, K., Scaling law of seismic spectrum, *J. Geophys. Res.*, **72**, 1217–1231, 1967.
- Aki, K., Scaling law of earthquake source time-function, *Geophys. J. Roy. Astron. Soc.*, **31**, 3–25, 1972.
- Anderson, R. N., and J. G. Sclater, Topography and evolution of the east Pacific rise between 5°S and 20°S, *Earth Planet. Sci. Lett.*, **14**, 433–442, 1972.
- Anderson, R. N., D. W. Forsyth, P. Molnar, and J. Mammertx, Fault plane solutions of earthquakes on the Nazca plate boundaries and the Easter plate, *Earth Planet. Sci. Lett.*, **24**, 188–202, 1974.
- Bonatti, E., and J. Honnorez, Sections of the earth's crust in the equatorial Atlantic, *J. Geophys. Res.*, **81**, 4104–4116, 1976.
- Brace, W. F., and J. D. Byerlee, California earthquakes: Why only shallow focus?, *Science*, **168**, 1573–1575, 1970.
- Brune, J. N., Seismic moment, seismicity and rate of slip along major fault zones, *J. Geophys. Res.*, **73**, 777–784, 1968.
- Brune, J. N., and C. Y. King, Excitation of mantle Rayleigh waves of period 100 seconds as a function of magnitude, *Bull. Seismol. Soc. Amer.*, **57**, 1355–1365, 1967.
- Burr, N. C., The relationship of source parameters of oceanic transform earthquakes to plate velocity and transform length, S.M. thesis, 87 pp., Mass. Inst. of Technol., Cambridge, 1977.
- Collette, B. J., H. Schouten, K. Rutten, and A. P. Sloopweg, Structure of the mid-Atlantic ridge province between 12° and 18°N, *Mar. Geophys. Res.*, **2**, 143–179, 1974.
- Davies, G. F., and J. N. Brune, Regional and global fault slip rates from seismicity, *Nature Phys. Sci.*, **229**, 101–107, 1971.
- Duschenes, J. D., and S. C. Solomon, Shear wave travel time residuals from oceanic earthquakes and the evolution of oceanic lithosphere, *J. Geophys. Res.*, **82**, 1985–2000, 1977.
- Fisher, R. L., J. G. Sclater, and D. P. McKenzie, Evolution of the central Indian ridge, western Indian Ocean, *Geol. Soc. Amer. Bull.*, **82**, 533–562, 1971.
- Forsyth, D. W., Mechanisms of earthquakes and plate motions in the east Pacific, *Earth Planet. Sci. Lett.*, **17**, 189–193, 1972.
- Forsyth, D. W., Anisotropy and the structural evolution of the oceanic upper mantle, Ph.D. thesis, 254 pp., Mass. Inst. of Technol., Cambridge, 1973.
- Forsyth, D. W., Fault plane solutions and the tectonics of the South Atlantic and Scotia Sea, *J. Geophys. Res.*, **80**, 1429–1443, 1975.
- Forsyth, D. W., and F. Press, Geophysical tests of petrological models of the spreading lithosphere, *J. Geophys. Res.*, **76**, 7963–7979, 1971.
- Fox, P. J., E. Schreiber, H. Rowlett, and K. McCamy, The geology of the Oceanographer fracture zone: A model for fracture zones, *J. Geophys. Res.*, **81**, 4117–4128, 1976.
- Geller, R. J., and H. Kanamori, Magnitudes of great shallow earth-

- quakes from 1904 to 1952, *Bull. Seismol. Soc. Amer.*, *67*, 587-598, 1977.
- Gutenberg, B., and C. F. Richter, Earthquake magnitude, intensity, energy and acceleration, *Bull. Seismol. Soc. Amer.*, *32*, 163-191, 1942.
- Gutenberg, B., and C. F. Richter, *Seismicity of the Earth and Associated Phenomena*, 2nd ed., Princeton University Press, Princeton, N. J., 1954.
- Gutenberg, B., and C. F. Richter, Earthquake magnitude, intensity, energy and acceleration, *Bull. Seismol. Soc. Amer.*, *46*, 105-145, 1956.
- Herron, E. M., Sea-floor spreading and the Cenozoic history of the east-central Pacific, *Geol. Soc. Amer. Bull.*, *83*, 1671-1685, 1972a.
- Herron, E. M., Two small crustal plates in the South Pacific near Easter Island, *Nature Phys. Sci.*, *240*, 39-47, 1972b.
- Isacks, B., J. Oliver, and L. R. Sykes, Seismology and the new global tectonics, *J. Geophys. Res.*, *73*, 5855-5899, 1968.
- Kanamori, H., and G. S. Stewart, Mode of the strain release along the Gibbs fracture zone, mid-Atlantic ridge, *Phys. Earth Planet. Interiors*, *11*, 312-332, 1976.
- Klitgord, K. D., J. D. Mudie, P. A. Larson, and J. Grow, Fast sea floor spreading on the Chile ridge, *Earth Planet. Sci. Lett.*, *20*, 93-99, 1973.
- Knopoff, L., Energy release in earthquakes, *Geophys. J. Roy. Astron. Soc.*, *1*, 44-52, 1958.
- Madariaga, R., Implications of stress-drop models of earthquakes for the inversion of stress drop from seismic observations, *Pure Appl. Geophys.*, *115*, 301-316, 1977.
- Mammerickx, J., R. N. Anderson, H. W. Menard, and S. M. Smith, Morphology and tectonic evolution of the east-central Pacific, *Geol. Soc. Amer. Bull.*, *86*, 111-118, 1975.
- McKenzie, D. P., and J. G. Slater, The evolution of the Indian Ocean since the Late Cretaceous, *Geophys. J. Roy. Astron. Soc.*, *24*, 437-528, 1971.
- Minster, J. B., T. H. Jordan, P. Molnar, and E. Haines, Numerical modeling of instantaneous plate tectonics, *Geophys. J. Roy. Astron. Soc.*, *36*, 541-576, 1974.
- Molnar, P., T. Atwater, J. Mamerickx, and S. M. Smith, Magnetic anomalies, bathymetry and the tectonic evolution of the South Pacific since Late Cretaceous, *Geophys. J. Roy. Astron. Soc.*, *40*, 383-420, 1975.
- Norton, I. O., The present relative motion between Africa and Antarctica, *Earth Planet. Sci. Lett.*, *33*, 219-230, 1976.
- Olivet, J., X. LePichon, S. Monti, and B. Sichel, Charlie-Gibbs fracture zone, *J. Geophys. Res.*, *79*, 2059-2072, 1974.
- Prothero, W. A., I. Reid, M. S. Reichle, and J. N. Brune, Ocean bottom seismic measurements on the east Pacific rise and Rivera fracture zone, *Nature*, *262*, 121-124, 1976.
- Reichle, M. S., G. F. Sharman, and J. N. Brune, Sonobuoy and teleseismic study of Gulf of California transform fault earthquake sequences, *Bull. Seismol. Soc. Amer.*, *66*, 1623-1641, 1976.
- Richardson, R. M., and S. C. Solomon, Apparent stress and stress-drop for intraplate earthquakes and tectonic stress in the plates, *Pure Appl. Geophys.*, *115*, 317-331, 1977.
- Rothé, J. P., *The Seismicity of the Earth*, 336 pp., Unesco, Paris, 1969.
- Saemundsson, K., Evolution of the axial rifting zone in northern Iceland and the Tjörnes fracture zone, *Geol. Soc. Amer. Bull.*, *85*, 495-504, 1974.
- Savage, J. C., and R. O. Burford, Discussion of paper by C. H. Scholz and T. J. Fitch, 'Strain accumulation along the San Andreas fault,' *J. Geophys. Res.*, *76*, 6469-6479, 1971.
- Slater, J. G., and R. L. Fisher, Evolution of the east central Indian Ocean, with emphasis on the tectonic setting of the Ninetyeast ridge, *Geol. Soc. Amer. Bull.*, *85*, 683-702, 1974.
- Slater, J. G., C. Bowin, R. Hey, H. Hoskins, J. Pierce, J. Phillips, and C. Tapscott, The Bouvet triple junction, *J. Geophys. Res.*, *81*, 1857-1869, 1976.
- Sleep, N. H., Formation of oceanic crust: Some thermal constraints, *J. Geophys. Res.*, *80*, 4037-4042, 1975.
- Solomon, S. C., Shear wave attenuation and melting beneath the Mid-Atlantic ridge, *J. Geophys. Res.*, *78*, 6044-6059, 1973.
- Solomon, S. C., Sizes of ridge crest earthquakes and lithospheric thickness at spreading centers (abstract), *Eos Trans. AGU*, *57*, 954, 1976.
- Solomon, S. C., and B. R. Julian, Seismic constraints on ocean-ridge mantle structure: Anomalous fault-plane solutions from first motions, *Geophys. J. Roy. Astron. Soc.*, *38*, 265-285, 1974.
- Stesky, R. M., W. F. Brace, D. K. Riiey, and P.-Y. F. Robin, Friction in faulted rock at high temperature and pressure, *Tectonophysics*, *23*, 177-203, 1974.
- Sykes, L. R., Mechanism of earthquakes and nature of faulting on mid-oceanic ridges, *J. Geophys. Res.*, *72*, 2131-2153, 1967.
- Thatcher, W., Strain accumulation on the northern San Andreas fault zone since 1906, *J. Geophys. Res.*, *80*, 4872-4880, 1975.
- Thompson, G., and W. Melson, The petrology of oceanic crust across fracture zones in the Atlantic Ocean: Evidence of a new kind of sea floor spreading, *J. Geol.*, *80*, 526-538, 1972.
- Tsai, Y. B., Determination of focal depth of earthquakes in mid-oceanic ridges from amplitude spectra of surface waves, Ph.D. thesis, 144 pp., Mass. Inst. of Technol., Cambridge, 1969.
- Udias, A., Source parameters of earthquakes from spectra of Rayleigh waves, *Geophys. J. Roy. Astron. Soc.*, *22*, 353-376, 1971.
- van Andel, T. H., D. K. Rea, R. P. Von Herzen, and H. Hoskins, Ascension fracture zone, Ascension Island and the mid-Atlantic ridge, *Geol. Soc. Amer. Bull.*, *84*, 1927-1956, 1973.
- Vogt, P. R., and G. L. Johnson, Transform faults and longitudinal flow below the midoceanic ridge, *J. Geophys. Res.*, *80*, 1399-1428, 1975.
- Weidner, D., and K. Aki, Focal depth and mechanism of midoceanic ridge earthquakes, *J. Geophys. Res.*, *78*, 1818-1831, 1973.
- Weissel, J. K., and D. E. Hayes, Magnetic anomalies in the southeast Indian Ocean, *Antarctic Oceanology II: The Australian-New Zealand Sector*, *Antarctic Res. Ser.*, vol. 19, edited by D. E. Hayes, pp. 165-196, AGU, Washington, D. C., 1972.
- Wilson, J. T., A new class of faults and their bearing on continental drift, *Nature*, *207*, 343-347, 1965.
- Wyss, M., Apparent stresses of earthquakes on ridges compared to apparent stresses of earthquakes in trenches, *Geophys. J. Roy. Astron. Soc.*, *19*, 479-484, 1970.

(Received June 22, 1977;
revised October 20, 1977;
accepted November 17, 1977.)

UNCLASSIFIED

SECURITY CLASSIFICATION OF THIS PAGE (When Data Entered)

REPORT DOCUMENTATION PAGE		READ INSTRUCTIONS BEFORE COMPLETING FORM
1. REPORT NUMBER AFOSR/TR-78-1016	2. GOVT ACCESSION NO.	3. RECIPIENT'S CATALOG NUMBER
4. TITLE (and Subtitle) THE RELATIONSHIP OF SOURCE PARAMETERS OF OCEANIC TRANSFORM EARTHQUAKES TO PLATE VELOCITY AND TRANSFORM LENGTH		5. TYPE OF REPORT & PERIOD COVERED Interim
7. AUTHOR(s) Norman C. Burr Sean C. Solomon		8. CONTRACT OR GRANT NUMBER(s) F44620-75-C-0064
9. PERFORMING ORGANIZATION NAME AND ADDRESS Massachusetts Institute of Technology Cambridge, MA 02139		10. PROGRAM ELEMENT, PROJECT, TASK AREA & WORK UNIT NUMBERS 62701E AO 1827-10
11. CONTROLLING OFFICE NAME AND ADDRESS Advanced Research Projects Agency/NMR 1400 Wilson Blvd. Arlington, VA 22209		12. REPORT DATE March 1978
14. MONITORING AGENCY NAME & ADDRESS (if different from Controlling Office) Air Force Office of Scientific Research/NP Bolling Air Force Base, Bldg. 410 Washington, DC 20332		13. NUMBER OF PAGES 12
		15. SECURITY CLASS. (of this report) UNCLASSIFIED
		15a. DECLASSIFICATION/DOWNGRADING SCHEDULE
16. DISTRIBUTION STATEMENT (of this Report) Approved for public release; distribution unlimited		
17. DISTRIBUTION STATEMENT (of the abstract entered in Block 20, if different from Report) UNCLASSIFIED		
18. SUPPLEMENTARY NOTES Journal of Geophysical Research, V83, p. 1193-1205, 1978.		
19. KEY WORDS (Continue on reverse side if necessary and identify by block number) source parameters, transform faults, thermal properties, mechanical properties		
20. ABSTRACT (Continue on reverse side if necessary and identify by block number) The source parameters of large earthquakes on oceanic transform faults are closely related to the thermal and mechanical properties of oceanic lithosphere. Several characteristics of these earthquakes (including magnitude, moment, and apparent stress) are synthesized according to local plate velocity V , ridge-ridge offset L , and average fault width W estimated by Brune's method. Several relationships result: (1) the maximum moment on a transform decreases with V , (2) maximum M_0 appears to increase with L for $L < 40$ km and may decrease for greater offsets, (3) apparent stress does not clearly depend on		

DD FORM 1473
1 JAN 73

EDITION OF 1 NOV 65 IS OBSOLETE

UNCLASSIFIED

SECURITY CLASSIFICATION OF THIS PAGE (When Data Entered)

UNCLASSIFIED

SECURITY CLASSIFICATION OF THIS PAGE(When Data Entered)

either V or L, (4) the maximum estimated $W(V)$ decreases with V, (5) the minimum estimated $W(L)$ increases with L, and (6) the largest earthquakes on long transforms occur near the transform center. Most of these relationships are consistent with the hypothesis that seismic failure occurs only at temperatures below a fixed value. An inversion of slip rate and magnitude data by transform supports this hypothesis and gives an estimate for the nominal temperature of the boundary separating stick slip and stable sliding. Though the actual thermal structure around oceanic transforms is not known, the idealized spreading plate models used in the inversion give a temperature range for the brittle to ductile boundary of 75° - 150° C. If possible uncertainties in the thermal structure are allowed for, a range of 50° - 300° C provides a conservative bound on the true limiting temperature. These temperature ranges are consistent with focal depths of transform earthquakes and with laboratory measurements of fault slip in rocks of compositions that are representative candidates for the material being faulted in oceanic transforms.

UNCLASSIFIED

SECURITY CLASSIFICATION OF THIS PAGE(When Data Entered)